Step 5. If $\varphi_2(t_f) > T_f + \varepsilon$, then b: = τ; proceed to Step 2.

Step 6. If $\varphi_2(t_f) < T_f - \varepsilon$, then a: = τ; proceed to Step 2.

Step 7. If $|\varphi_2(t_f) - T_f| \leq \varepsilon$, set $t_2 = (a + b)/2$; the calculation is over.

NOTATION

t, time; T(t), temperature of metal at time t; $T_c(t)$, temperature of medium at time t; k', reduced form factor of body; α, convective thermoemission coefficient; σ, radiative thermoemission coefficient; T_0 and T_f, initial and final temperature of metal; t_f, fixed duration of heating process; β, ratio of activation energy to gas constant; κ, specified constant characterizing the dynamics of skin growth; A_1, A_2, minimum and maximum temperature of medium; k, form factor of body; R, characteristic dimension of body; c, specific heat; ρ, density of material.

LITERATURE CITED

1. V. B. Kovalevskii, V. I. Panasyuk, and O. Yu. Sedyako, Inzh.-fiz. Zh., 59, No. 1, 168-169 (1990); Paper 1226-V90 Deposited at VINITI [in Russian], Moscow (1990).
2. A. V. Kavaderov and Yu. A. Samoilovich, Inzh.-fiz. Zh., No. 7, 110-113 (1959).

HEAT TRANSFER ON MOUNTING ELECTRONIC COMPONENTS ONTO A PRINTED CIRCUIT BOARD

V. G. Prokopov, N. M. Fialko, V. G. Sarioglo, and A. A. Grachev

UDC 621.3.049.75.002

The results of mathematical modeling of nonlinear nonsteady heat-transfer processes in conditions of IR soldering of components onto printed circuit boards are outlined.

Establishing the thermophysical principles of the technological process of mounting electronic components on a printed circuit board (PB) is an urgent problem in the development of this technology [1-3]. Mathematical modeling plays an important role in solving this problem, because of its many well-known advantages: the possibility of compensating for the unavoidable omissions of experimental work, significant reduction in the volume of expensive full-scale experiments, the simplicity of investigating different parameter combinations, etc.

The aim of the present work is the mathematical modeling of heat transfer in the technology of surface mounting. The physical situation corresponding to the use of resistive and IR heating is analyzed. The temperature conditions of printed elements (PE) corresponding to all the possible single electronic-engineering components (EEC) which may be mounted on PB of highly and poorly heat-conducting materials are studied. Thus, outputless EEC (a monolithic tantalum capacitor and a matrix microframe) and EEC with planar outputs (an N-type microframe and a plastic frame) are considered, in the process of mounting on ceramic and glass-textolite PB.

In characterizing the processes that occur overall in the given conditions, a series of factors complicating the investigation may be noted: in particular, nonlinearities of various kinds, complex configurations of the given regions, phase transitions (melting and hardening of the solder), PE Motion in the furnace for IR soldering, diversity of the PE constructional materials, etc. Consequently, the preliminary investigations must include

Institute of Engineering Thermal Physics, Academy of Sciences of the Ukrainian SSR, Kiev.

Translated from Inzhenerno-fizicheskii Zhurnal, Vol. 61, No. 2, pp. 204-210, August, 1991. Original article submitted August 10, 1990.

0022-0841/91/6102-0959$12.50

full-scale experiments and their comparison with data obtained in various mathematical models of the process. This comparison provides the basis for the choice of the relatively simple mathematical model outlined below, which corresponds adequately to the real thermal situation.

Accordingly, the physical formulation of the problem is now described. The PE moves at constant velocity V in the furnace for IR soldering. The construction of the furnace is such that zones characterized by different heat-transfer conditions of the PE with the furnace may be distinguished. These zones are considered separately for the upper and lower PE surfaces. For the lower surface, six zones may be distinguished: in the first and second, there is preliminary resistive heating of the PE: in the third, resistive heating accompanies the IR treatment of the upper PE surface; the fourth zone, which is relatively small, is a heat-insulated section; in the fifth and sixth zones, there is heat extraction with boundary conditions of the third kind. For the upper PE surface, the division into zones is as follows. Zone 1* is characterized by the presence of convective and radiative heat transfer of the upper board surface with the air and with the walls of the channel formed by the furnace roof and the transporter, respectively. This zone, in turn, may be divided into two subzones 1*a and 1*b, in view of the different heating conditions of the air and the channel walls determined by the autonomous resistive heaters in each of the subregions. Zone 2* corresponds to IR heating of the PE, and may be divided into three subregions 2*a, 2*b, and 2*c. In subregion 2*a, end effects associated with the IR-heater construction (the lack of heat insulation at the end surfaces) are significant. This subregion corresponds to a small initial portion of the IR-heating section; the remainder of this section corresponds to subregion 2*b. Subregion 2*c is determined by the presence of the second IR-heating section.

The boundary conditions at the PE boundary surfaces correspond to this heat-transfer pattern in the various zones of the furnace. Heat flow to the PE in the direction perpendicular to its motion in the flow is ignored.

Without loss of generality in formulating the mathematical models, the Stefan problem for an N-type microframe mounted on a PB in conditions of resistive and IR heating is taken as a specific example (Fig. 1):

$$\frac{\partial}{\partial x}\left[\lambda(x,\ y)\frac{\partial t}{\partial x}\right]+\frac{\partial}{\partial y}\left[\lambda(x,\ y)\frac{\partial t}{\partial y}\right]-L\rho\delta^{*}(t-t_{f})\frac{\partial t}{\partial\tau}=c_{v}(x,\ y)\frac{\partial t}{\partial\tau}, \qquad (1)$$

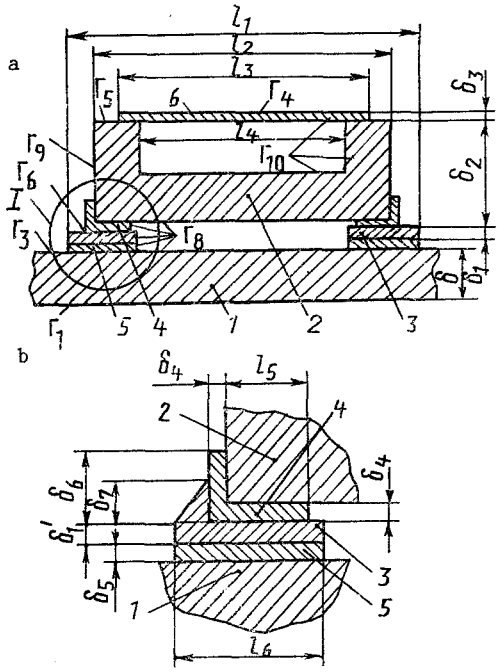

Fig. 1. Formulation of the problem: a) general view of PE; b) solder joint; 1) printed-circuit board; 2) frame base; 3) solder; 4) output; 5) contact area; 6) lid of frame.

$x,\ y \in \Omega$ when $0 < \tau \leqslant \tau_f$; $x,\ y \in \bar{\Omega}$ when $\tau_f < \tau \leqslant \tau_6$;

$$\left.\frac{\partial t}{\partial n}\right|_{\Gamma_1} =$$

$$= \begin{cases} 0 & \text{when } 0 < x \leqslant V\tau,\ 0 < \tau \leqslant \tau^*; \\ -\dfrac{q_1}{\lambda} & \begin{cases} \text{when } V\tau < x < l,\ 0 < \tau \leqslant \tau^*; \\ \text{when } 0 < x < l,\ \tau^* < \tau \leqslant \tau_1; \\ \text{when } 0 < x \leqslant V(\tau - \tau_1),\ \tau_1 < \tau \leqslant (\tau_1 + \tau^*); \end{cases} \\ -\dfrac{q_2}{\lambda} & \begin{cases} \text{when } 0 < x \leqslant V(\tau - \tau_2),\ \tau_2 < \tau \leqslant (\tau_2 + \tau^*); \\ \text{when } V(\tau - \tau_1) < x < l,\ \tau_1 < \tau \leqslant (\tau_1 + \tau^*); \\ \text{when } 0 < x < l,\ (\tau_1 + \tau^*) < \tau \leqslant \tau_2; \end{cases} \\ -\dfrac{q_3}{\lambda} & \begin{cases} \text{when } V(\tau - \tau_2) < x < l,\ \tau_2 < \tau \leqslant (\tau_2 + \tau^*); \\ \text{when } 0 < x < l,\ (\tau_2 + \tau^*) < \tau \leqslant \tau_3; \\ \text{when } 0 < x \leqslant V(\tau - \tau_3),\ \tau_3 < \tau \leqslant \tau_4; \\ \text{when } 0 < x \leqslant [l - V(\tau - \tau_3)],\ \tau_4 < \tau \leqslant (\tau_3 + \tau^*); \end{cases} \\ 0 & \begin{cases} \text{when } V(\tau - \tau_3) < x < l,\ \tau_3 < \tau \leqslant \tau_4; \\ \text{when } [l - V(\tau - \tau_3)] < x \leqslant V(\tau - \tau_4),\ \tau_4 < \tau \leqslant (\tau_3 + \tau^*); \\ \text{when } 0 < x \leqslant [l - V(\tau - \tau_4)],\ (\tau_3 + \tau^*) < \tau \leqslant (\tau_4 + \tau^*); \end{cases} \\ \dfrac{\alpha_1}{\lambda}(t - t_{c_1}) & \begin{cases} \text{when } [l - V(\tau - \tau_4)] < x < l,\ (\tau_3 + \tau^*) < \tau \leqslant (\tau_4 + \tau^*); \\ \text{when } 0 < x < l,\ (\tau_4 + \tau^*) < \tau \leqslant \tau_5; \\ \text{when } 0 < x \leqslant V(\tau - \tau_5),\ \tau_5 < \tau \leqslant (\tau_5 + \tau^*); \end{cases} \\ \dfrac{\alpha_2}{\lambda}(t - t_{c_2}) & \begin{cases} \text{when } V(\tau - \tau_5) < x < l,\ \tau_5 < \tau \leqslant (\tau_5 + \tau^*); \\ \text{when } 0 < x < l,\ (\tau_5 + \tau^*) < \tau \leqslant \tau_6; \end{cases} \end{cases} \tag{2}$$

$$\left.\frac{\partial t}{\partial n}\right|_{\Gamma_i} = \begin{cases} 0 & \text{when } 0 < x \leqslant V\tau,\ 0 < \tau \leqslant \tau^*; \\ -\dfrac{\alpha^*_{1\Gamma_i}}{\lambda}(t - t_{w_1}) & \begin{cases} \text{when } V\tau < x < l,\ 0 < \tau \leqslant \tau^*; \\ \text{when } 0 < x < l,\ \tau^* < \tau \leqslant \bar{\tau}_1; \\ \text{when } 0 < x \leqslant V(\tau - \bar{\tau}_1),\ \bar{\tau}_1 < \tau \leqslant (\bar{\tau}_1 + \tau^*); \end{cases} \\ -\dfrac{\alpha^*_{2\Gamma_i}}{\lambda}(t - t_{w_2}) & \begin{cases} \text{when } V(\tau - \bar{\tau}_1) < x < l,\ \bar{\tau}_1 < \tau \leqslant (\bar{\tau}_1 + \tau^*); \\ \text{when } 0 < x < l,\ (\bar{\tau}_1 + \tau^*) < \tau \leqslant \bar{\tau}_2; \end{cases} \end{cases} \tag{3}$$

$i = 3,\ 4,\ 5,\ 6;$

$$\left.\frac{\partial t}{\partial n}\right|_{\Gamma_i} = 0, \tag{4}$$

$i = 7,\ 8,\ 9,\ 10;$

$$t|_{\tau=0} = t_0. \tag{5}$$

In Eq. (3), $\alpha_{1\Gamma_i}^* = \alpha_{1_{co}}^* + \alpha_{1,i_r}^*$; $\alpha_{2\Gamma_i}^* = \alpha_{2co}^* + \alpha_{2,i_r}^*$; $\alpha_{1_{co}}^*$ and $\alpha_{2_{co}}^*$ are found in accordance with the equation for the effective heat-transfer coefficient in a close horizontal air layer [4]. In the time interval corresponding to PE passage through the section of furnace $X_7 < X < X_8$, $\alpha_{2_{co}}^* = 0$. According to [5]

$$\alpha^*_{1,i_r} = c_0\varepsilon_{1,i}\left[\left(\frac{t+273}{100}\right)^4_{\Gamma_i} - \left(\frac{t_{w_1}+273}{100}\right)^4\right] \Big/ (t - t_{w_1})_{\Gamma_i},$$

$$\alpha^*_{2,i_r} = c_0\varepsilon_{2,i}\left[\left(\frac{t+273}{100}\right)^4_{\Gamma_i} - \left(\frac{t_{w_2}+273}{100}\right)^4\right] \Big/ (t - t_{w_2})_{\Gamma_i}.$$

The finite-element method is used to solve Eqs. (1)-(5) [6-8]. Characteristic results of the numerical experiments corresponding to the initial parameters: $X_1 = 0.25$ m; $X_2 = 0.5$ m; $X_3 = 0.67$ m; $X_4 = 0.68$ m; $X_5 = 0.81$ m; $X_6 = 1.0$ m; $X_7 = 0.525$ m; $X_8 = 0.75$ m; $\ell = 5\cdot10^{-2}$m; $\ell_1 = 8.45\cdot10^{-3}$ m; $\ell_2 = 6.8\cdot10^{-3}$ m; $\ell_3 = 5.55\cdot10^{-3}$ m; $\ell_4 = 4.575\cdot10^{-3}$ m; $\ell_5 = 0.75\times10^{-3}$ m; $\ell_6 = 1.625\cdot10^{-3}$ m; $\delta_1 = 0.3\cdot10^{-3}$ m; $\delta_2 = 2.5\cdot10^{-3}$ m; $\delta_3 = 0.2\cdot10^{-3}$ m; $\delta_4 = 0.2\cdot10^{-3}$ m; $\delta_5 = 0.15\cdot10^{-3}$ m; $\delta_6 = 0.7\cdot10^{-3}$ m; $\delta_7 = 0.5\cdot10^{-3}$ m; $t_0 = 20°C$; $t_{c_1} = 30°C$; $t_{c_2} = 20°C$;

t_f = 183°C; V = $6 \cdot 10^{-3}$ m/sec, α_1 = 20 W/m²·K; α_2 = 45 W/m²·K; $\alpha_{1_{co}}$* = 7.9 W/m²·K; $\alpha_{2_{co}}$* = 7.1 W/m²·K, and $\delta_1' = 0.2 \cdot 10^{-3}$ m are as follows:

$$t_{w_1} = \begin{cases} 50 + 180X & \text{when } 0 < X \leqslant X_1; \\ 80 + 60X & \text{when } X_1 < X \leqslant X_2; \end{cases}$$

$$t_{w_2} = \begin{cases} 9600X - 4690 & \text{when } X_2 < X \leqslant X_7; \\ 350\ ^\circ\text{C} & \text{when } X_7 < X \leqslant X_8; \\ 1340 - 1320X & \text{when } X_8 < X \leqslant X_6; \end{cases}$$

q_1 = 6500 W/m², q_2 = 8000 W/m², q_3 = 17,500 W/m², c_0 = 5.67 W/m²·K⁴, L = 47,312 J/kg. Table 1 gives the values of λ, c_p, and ρ.

To elucidate the basic variation in the PE thermal state, heat transfer in the PB itself, in the microframe, and in the solder is considered systematically. Typical results are shown in Figs. 2-5.

First note the characteristic features of the PB thermal state. The dependence $t = f(\tau)$ at fixed points of the lower PB surface is shown in Fig. 2. As is evident, at the given points of the PB, the temperature variation over time is extremal in character. The greatest temperature peak corresponds to the rear PB edge and the smallest to the central region; the difference is 27°C. It is noteworthy that the extremum of the temperature curves is expressed sufficiently clearly for points corresponding to the front and rear edges of the PB (curves 1 and 3). In the central part of the PB (curve 2), high temperature levels which are close to the maximum are observed over a relatively large time interval ($113 \lesssim \tau \lesssim 140$ sec).

The time dependence of the temperature drop Δt over the PB thickness is now briefly considered (Fig. 3). As is evident from Fig. 3, Δt varies not only in magnitude but also in sign as the PE passes through the furnace. Thus, $\Delta t < 0$ in zones 1, 2, and 3. In zone 4 or the initial section of zone 5, change in sign of Δt is seen, so that $\Delta t > 0$ in the remaining zones. For points which are further away from the PB front edge, change in sign of Δt occurs later. Obviously, this behavior of Δt over time is a consequence of the specific heating and cooling conditions of the upper and lower PE surfaces as it moves in the furnace for IR soldering.

Turning to the basic features of the temperature variation in the peripheral microframe (MF), the temperature distribution at the upper t_u and lower t_ℓ MF surfaces is shown in Fig. 4. In describing the basic dynamic features of these temperatures, first note the change in their relative values. In resistive heating zones 1, 2, and 3, the temperature $t_\ell > t_u$ in MF regions adjacent to its ends and $t_\ell < t_u$ in the central part of the MF (curves 1, 2, 3). Over time, this pattern changes, and the opposite relation between t_ℓ and t_u close to the MF ends is seen even in zone 5. This is evidently due to the change in heating and cooling conditions in PE motion in the furnace channel. Thus, in zone 5, there is no resistive heating, and the lower PE surface is cooled, while the upper surface is heated on account of the IR emitter. The situation corresponding to $t_\ell < t_u$ in the central part of the MF is also observed in the initial section of zone 6. With further PE motion, the relation between these temperatures changes: the temperature of the MF upper surface becomes lower overall, i.e., $t_\ell > t_u$ in the central part of the frame (curve 5). This pattern is evidently associated with more intense cooling of the MF upper boundary surface in the given time interval on account of direct contact with the cooling medium. Note that the variation in t_ℓ and t_u close to the MF ends is determined to a considerable extent by the heat flow between the PB and the frame through its outputs.

TABLE 1. Thermophysical Properties of PE Constructional Elements

Constructional element	Material	λ, W/m·K	c_p, J/kg·K	ρ, kg/m³	ε
Board	Ceramic with metal coating	12,6	800	3800	0,5
Frame base	Ceramic	—	—	—	0,3
Lid	Nickel	81	470	8900	0,35
Output	Covar	19,3	670	8300	0,35
Contact area	Copper	384	400	8950	—
Solder	Pos-61	50,2	199	8540	—

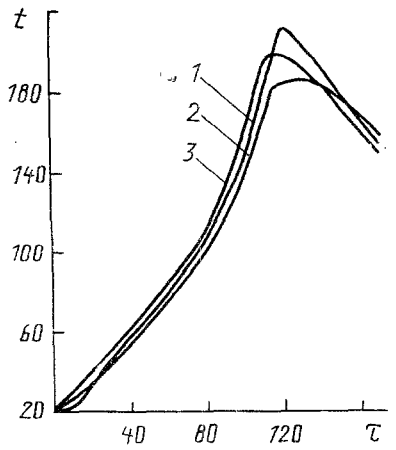

Fig. 2

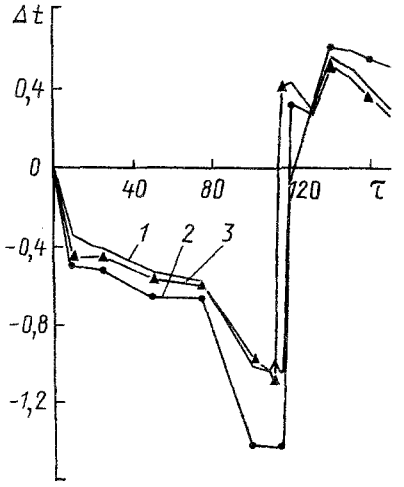

Fig. 3

Fig. 2. Variation in temperature over time at various points of lower surface of ceramic PB in the presence of a peripheral microframe: 1) x = 0; 2) $24.75 \cdot 10^{-3}$, 3) $50 \cdot 10^{-3}$ m. t, °C; τ, sec.

Fig. 3. Time distribution of Δt in various cross sections of ceramic PB in the presence of a peripheral microframe: 1) x = 0; 2) $24.75 \cdot 10^{-3}$; 3) $50 \cdot 10^{-3}$ m. Δt, °C.

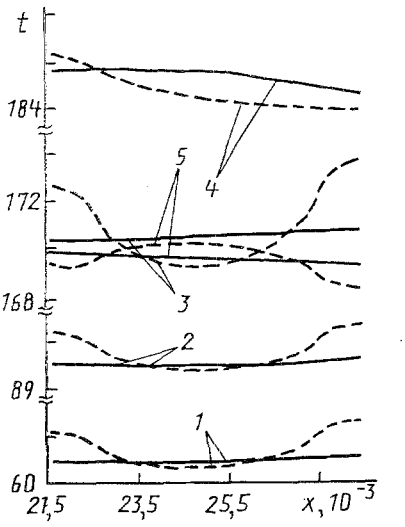

Fig. 4

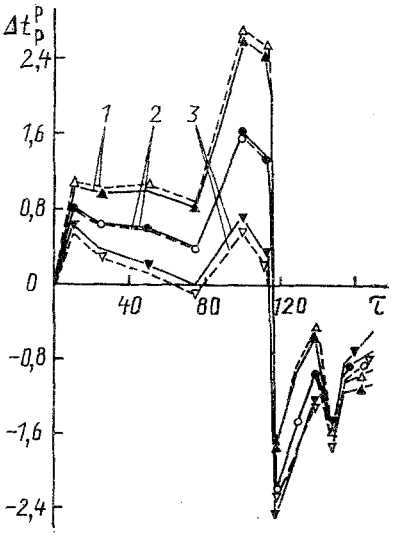

Fig. 5

Fig. 4. Temperature of upper (continuous curve) and lower (dashed curve) surfaces of peripheral microframe in ceramic PB at times τ = 50 (1), 75 (2), 112.5 (3), 120 (4), and 160 sec (5). x, m.

Fig. 5. Dependence $\Delta t_p^P = f(\tau)$ at various points of the upper (dashed line) and lower (continuous curve) surface of solder in the presence of peripheral microframe on ceramic PB: 1) points A, A'; 2) B, B'; 3) C, C'. Δt, °C.

Now consider the thermal state of the solder. The variation in Δt_p^P over time is shown in Fig. 5 for points A, B, C of the upper surface and A', B', C' of the lower surface of the solder; A, A', B, B', C, C' are points in vertical cross sections of the solder passing through its front (in the direction of motion) edge, center, and rear edge; $\Delta t_p^P(x, \tau) = t_1(x, \tau) - t_2(x + s, \tau)$, where $t_1(x, \tau)$, $t_2(x + s, \tau)$ are the temperatures of the first and second solder joints in the direction of PE motion at the corresponding points; s is

the distance between the corresponding points of solder joints 1 and 2, $s = 6.825 \cdot 10^{-3}$ m. In this case, the x coordinate of points A, A' for the first joint is $29.25 \cdot 10^{-3}$ m; of points B, B', $28.4375 \cdot 10^{-3}$ m; of points C, C', $27.625 \cdot 10^{-3}$ m. As is evident from Fig. 5, Δt_p^P is relatively small: no greater than 2.75°C. In the initial period, Δt_p^P is positive for a considerable time, i.e., the temperature of the first joint in the direction of PE motion is higher than that of the second. After a time, Δt_p^P becomes negative, i.e., the temperature of the second solder joint exceeds that of the first. Note that, on reaching maximum PE temperature levels (Fig. 2), Δt_p^P is negative. For this reason, it is expedient to determine the minimum heat supply required from the temperature of the first joint (in the direction of PE motion).

In summary, the mathematical modeling of the thermal state of printed elements in conditions of surface mounting using resistive and IR heating has been considered. Characteristic results obtained in analyzing numerical experiments have been outlined, and the basic heat-transfer laws in the given physical situation have been established.

NOTATION

t, t_0, current and initial temperature; t_{c_1}, t_{c_2}, temperature of medium in zones 5 and 6; t_{w_1}, t_{w_2}, temperature of upper channel wall of furnace in zones 1* and 2*; x, y, abscissa and ordinate of Cartesian coordiante system associated with PE: Ω, $\bar{\Omega}$, spatial region corresponding to PE before and after soldering; l, PE length; τ, time; τ^*, time in which PE traverses a distance equal to its length; τ_j, time in which the PE covers the distance from the beginning of the IR furnace to the end of the corresponding heat-transfer zone of the lower PE surface with the furnace, $j = 1, 2, \ldots, 6$, $\tau_j = X_j/V$; X_k, abscissa of upper boundary of heat-transfer zone of PE surface in the Cartesian coordinate system associated with the furnace, $k = 1, 2, \ldots, 8$; V, velocity of PE motion in furnace; $\bar{\tau}_1$, $\bar{\tau}_2$, time in which PE covers the distance from the beginning of the furnace to the end of the corresponding heat-transfer zone of the upper PE surface with the furnace, $\bar{\tau}_1 = \tau_2$, $\bar{\tau}_2 = \tau_6$; τ_f, time at which the volume-mean temperature of the solder reaches the melting point t_f; q_1, q_2, q_3, heat-flux density supplied; α_1, α_2, heat-transfer coefficients of convection in zones 5 and 6; Γ_i, sections of PE boundary surface, $i = 1, 2, \ldots, 10$ (Γ_7 corresponds to the PB end surface); $\alpha_{1\Gamma_i}{}^*$, $\alpha_{2\Gamma_i}{}^*$, total heat-transfer coefficients at section i of PE boundary surfaces in zones 1* and 2*; $\alpha_{1_{co}}{}^*$, $\alpha_{2_{co}}{}^*$, convective heat-transfer coefficients in zones 1* and 2*; c_0, emissivity of absolute black body; $\varepsilon_{1,i}$, $\varepsilon_{2,i}$, reduced emissivities of section i of PE boundary surfaces in zones 1* and 2*; λ, C_p, ρ, thermal conductivity, mass specific heat, and density of material; L, specific heat of crystallization of solder material; $\delta^*(t - t_f)$, Dirac delta function.

LITERATURE CITED

1. A. V. Egunov, B. L. Zhorzholiani, V. G. Zhuravskii, et al., Automation and Mechanization of the Assembly and Mounting of Elements on Printed Circuit Board [in Russian], Moscow (1988).
2. A. A. Grachev, A. I. Galushka, B. F. Koshevoi, et al., Mounting Microframes of Integral Circuits on Boards [in Russian], Reviews in Electronic Engineering, Ser. 7, TOPO, No. 4(1005), Moscow (1984).
3. D. Laimen, Élektronika, 59, No. 3, 52-60 (1986).
4. G. N. Dul'nev, Heat and Mass Transfer in Radioelectronic Equipment [in Russian], Moscow (1984).
5. R. Siegel and J. R. Howell, Thermal Radiation Heat Transfer, 2nd ed., McGraw-Hill, New York (1980).
6. O. Zenkevich and K. Morgan, Finite Elements and Approximation [Russian translation], Moscow (1986).
7. L. Segerlind, Application of Finite-Element Method [in Russian], Moscow (1979).
8. N. M. Fialko, V. G. Prokopov, V. G. Sarioglo, and A. A. Grachev, in: Heat and Mass Transfer in the Technology and Operation of Electronic and Microelectronic Systems: Proceedings of an International School and Seminar, Minsk, September 19-22, 1989 [in Russian] (1990), Part 2, pp. 30-39.